*Natural Resources Research, Vol. 30, No. 3, June 2021 (© 2021)*
https://doi.org/10.1007/s11053-021-09815-7

*Original Paper*

# Mechanical Behaviors of Granite After Thermal Treatment Under Loading and Unloading Conditions

**Zhennan Zhu,[1,2] Hong Tian,[1,2,6] Thomas Kempka,[3,4] Guosheng Jiang,[1,2] Bin Dou,[1,2] and Gang Mei[5]**

*Received 27 October 2020; accepted 14 January 2021*
*Published online: 30 January 2021*

Understanding the mechanical behaviors of granite after thermal treatment under loading and unloading conditions is of utmost relevance to deep geothermal energy recovery. In the present study, a series of loading and unloading triaxial compression tests (20, 40 and 60 MPa) on granite specimens after exposure to different temperatures (20, 200, 300, 400, 500 and 600 °C) was carried out to quantify the combined effects of thermal treatment and loading/unloading stress conditions on granite strength and deformation. Changes in the microstructure of granite exposed to high temperatures were revealed by optical microscopy. The experimental results indicate that both, thermal treatment and loading/unloading stress conditions, degrade the mechanical behaviors and further decrease the carrying capacity of granite. The gradual degradation of the mechanical characteristics of granite after thermal treatment is mainly associated with the evolution of thermal micro-cracks based on optical microscopy observations. The unloading stress state induces the extension of tension cracks parallel to the axial direction, and thus, the mechanical properties are degraded. Temperatures above 400 °C have a more significant influence on the mechanical characteristics of granite than the unloading treatment, whereby 400 °C can be treated as a threshold temperature for the delineation of significant deterioration. This study is expected to support feasibility and risk assessments by means of providing data for analytical calculations and numerical simulations on granite exposed to high temperatures during geothermal energy extraction.

**KEY WORDS:** Granite, Thermal treatment, Unloading, Mechanical properties, Micro-structure.

## INTRODUCTION

Clean and efficient energy is a direction of future energy development, and deep geothermal energy is recently identified as a renewable and alternative energy source (Pranay et al. 2019; Yu et al. 2020). After the first deep, hot dry rock (HDR) project being set up in Fenton Hill in 1973 in the U.S. (Duchane and Brown 2002), many enhanced geothermal system (EGS) research projects have been developed around the world up to now (Zhang et al. 2019). There are also abundant geothermal resources in China, especially in the Tibetan Pla-

[1]Faculty of Engineering, China University of Geosciences, Lumo Road 388, Wuhan 430074, China.
[2]National Center for International Research On Deep Earth Drilling and Resource Development, China University of Geosciences, Lumo Road 388, Wuhan 430074, China.
[3]Fluid Systems Modeling, Telegrafenberg, GFZ German Research Centre for Geosciences, 14473 Potsdam, Germany.
[4]University of Potsdam, Institute for Geosciences, Karl-Liebknecht-Str, 24-25, 14476 Potsdam, Germany.
[5]School of Engineering and Technology, China University of Geosciences, Xueyuan Road 29, Beijing 100083, China.
[6]To whom correspondence should be addressed; e-mail: htian@cug.edu.cn



1520-7439/21/0600-2733/0 © 2021 International Association for Mathematical Geosciences

teau. For example, the Gonghe Basin, located in the northeastern Tibetan Plateau, is one of the most favorable regions to build the first EGS in China (Gao et al. 2018). The surrounding rock in the aforementioned geothermal projects may experience high temperatures, and changes in the rock properties may induce instability after undergoing high temperatures. In addition, rock masses are often under an unloading confining stress state during and after drilling, which can also induce severe rock failures. Loading and unloading stress conditions may induce reactivation of existing faults, generation of fracture networks and even seismic events. Therefore, it is essential to understand the mechanism of the combined effect of high temperature and loading/unloading stress conditions on deep rocks for successful implementation of subsurface utilization projects such as those above.

In recent decades, extensive laboratory research has shown that thermal treatment has a substantial influence on mechanical properties and microstructures of rocks. In general, rock strength and deformation properties such as compressive strength, tensile strength, elastic modulus, fracture toughness and Poisson's ratio exhibit different levels of degradation and gradually decrease with increasing temperature. Nasseri et al. (2007) evaluated the influence of thermal damage on fracture toughness ($K_{IC}$) of Westerly granite, and found that thermal cracking significantly reduced $K_{IC}$ of their rock specimens. Singh et al. (2015) conducted compression tests on Bundelkhand granite and obtained the effect of temperature on uniaxial compressive strength (UCS). Water cooling and liquid nitrogen cooling decrease UCS and elastic modulus of granite (Jin et al. 2019; Wu et al. 2019b). Wu et al. (2019a) performed a series of Brazilian tests on granite after heating/cooling treatments with water and air cooling and found the tensile strength of the former is lower than that of the latter. Zhu et al. (2020) found that UCS and elastic modulus of granite decrease with thermal cycling, while the mechanical properties remain almost unchanged once the thermal cycles reach 20 times. Yang et al. (2020) carried out triaxial conventional compression experiments on Rizhao granite after exposure to high temperature, and their experimental results indicate that a thermal treatment of 450 °C was identified as the transition temperature that induces notable changes of granite mechanical properties (elastic modulus, peak strength and Poisson's ratio). The changing law of mechanical behavior after high temperature shows a similar response for other types of rocks, e.g., claystone (Tian et al. 2014), limestone (Gónzalez-Gómez et al. 2015), sandstone (Yang et al. 2017), marble (Zhu et al. 2018) and shale (Jiang et al. 2019).

Previous studies have shown that the deep degradation mechanism of mechanical and thermal properties of rocks after high temperature is mainly related to changes in mineral grains and mineral composition induced by elevated temperatures (Tian et al. 2014; Yang et al. 2017; Zhu et al. 2018). Clark (1966) reported that differences in the thermal expansion characteristics of minerals in the assemblage of mineral grains cause structural damage to the heated rocks and that differences in thermal expansion along different crystallographic axes of the same mineral also contribute to structural damage upon heating (Somerton 1993). The $\alpha$–$\beta$ phase transition of quartz at 573 °C at ambient pressures, accompanied by a linear expansion of 0.45%, can also cause structural changes upon heating of granite (Glover et al. 1995). Zhang et al. (2016) pointed out that the escape of various types of water can also induce structural damage, and the temperature ranges of vapourization of attached water, bound water and constitution water are room temperature to 100 °C, 100–300 °C and 300–500 °C, respectively. Changes in micro-structures have been verified by observations of thin sections of rock specimens after exposure to various temperatures through X-ray micro computed tomography (CT) (Mohamadi and Wan 2016; Fan et al. 2018), scanning electron microscopy (SEM) (Mahanta et al. 2016; Shen et al. 2018; Han et al. 2019) and optical microscopy (Peng et al. 2016; Rong et al. 2018). It was found that the microstructure of the rocks is greatly damaged by thermal treatment, especially in the evaluation of micro-cracks, which constantly initiate, propagate and coalesce with increasing thermal treatment temperature.

However, the experimental studies mentioned above were mainly conducted under loading conditions, under which the deformation characteristics and mechanical behaviors of rocks are essentially different from those during deep underground excavation, where the wall rocks always undergo stress release (Lau and Chandler 2004). A great number of researchers has experimentally investigated the mechanical properties of rocks under unloading, mainly focusing on the failure modes (Zhao et al. 2015; Dai et al. 2018), unloading rates (Huang et al. 2017), energy evolution (Li et al. 2017;

Chen et al. 2018), acoustic emission characteristics (Liang et al. 2017) and lateral deformation (Chen et al. 2016).

Although the effects of thermal treatment and loading/unloading stress conditions on rock mechanical properties have been demonstrated separately, limited publications (Ding et al. 2016; Meng et al. 2018) combining the two aspects are available, which mainly focus on sandstone. It has been found through exploratory geothermal well tests that deep granite strata have adequate temperatures to serve as geothermal reservoirs (Fox et al. 2013). Therefore, it is essential to pay attention to the mechanical properties of granite subjected to the extreme boundary conditions of HDR projects. Therefore, we conducted a series of loading and unloading triaxial compression tests on granite specimens, exposed to various temperatures to understand the combined effects of thermal treatment and loading/unloading and stress condition evolution. The evolution of the microstructure of the granite after exposure to high temperatures was revealed by optical microscopy. These experimental results will support feasibility and risk assessments by means of providing data for analytical calculations and numerical simulations of granite exposed to high temperatures during geothermal energy extraction.

## EXPERIMENTAL DESIGN

### Description of Rock Specimens

All of the experiments were conducted on granite mined from a mine with a depth of 200 m located in Nanan city, Fujian Province, in the southeastern region of China. The specimens were reddish-brown in color and fine-grained (Fig. 1). The mineral composition of the tested granite was 41.42% potash feldspar, 30.79% soda feldspar, 15.90% biotite and 11.89% quartz, according to petrophysical analysis using X-ray diffraction. The rock was processed into cylinders of 100 mm in length and 50 mm in diameter according to the method suggested by ISRM (Ulusay and Hudson 2007). The measured density and P-wave velocity were $2.596 \pm 0.003$ g/cm$^3$ and $4167 \pm 200$ m/s, respectively.

### Experimental Procedures

In this research, the P-wave velocities of the specimens were measured before and after the thermal treatments, and then loading/unloading compression testing as well as optical microscopy observation was conducted on the heated ones. The specimens were first heated to a target temperature of 105 °C, and the target temperature was held for 24 h before the specimens were cooled to room temperature in a dryer to remove all moisture content. Currently, HDR temperature ranges from 150 °C to 500 °C within 5–6 km depths (Breede et al. 2013). Thus, the maximal design temperature in the present study was 600 °C. Next, the specimens were subjected to elevated temperatures of 200, 300, 400, 500 and 600 °C in a SG-XL1200 high-temperature box furnace using a modest heating rate of 5 °C/min to minimize the thermal gradient and thermal shock within the rock. This heating rate has been previously employed in several successful experiments (Ding et al. 2016; Yang et al. 2017; Rathnaweera et al. 2018; Shen et al. 2018; Wu et al. 2019a, 2019b). Wang et al. (2020) have checked that 1 h was enough for a uniform temperature distribution across the granite sample applying heat flux on the complete outer surfaces. Therefore, the target temperature was then maintained for 2 h to ensure that the specimens were heated adequately. Thereafter, the specimens were naturally cooled to room temperature in the furnace chamber, and then placed in a desiccator before the mechanical tests to reduce the effect of moisture content in the air. The P-wave velocities of the specimens were measured before and after high temperature using an RSM-SY5 (T) ultrasonic tester (Fig. 2). An optical microscope (DM 2500P) was used to observe the micro-structural characteristics of the granite after its exposure to various temperatures (Fig. 2).

Loading triaxial compression and unloading confining pressure tests were performed using an electro-hydraulic servo-controlled rock mechanics testing system (TAW-2000) with a maximum loading capacity of 2000 kN and a maximum confining pressure of 80 MPa (Figure 2). The stress conditions for the two testing types are illustrated in Figure 3. Three different initial confining pressures (i.e., 20, 40 and 60 MPa) were chosen for the two types of tests. For the loading condition determination, conventional uniaxial and triaxial compression tests were conducted under axial displacement control until failure at a rate of 0.005 mm/s, with the hydrostatic

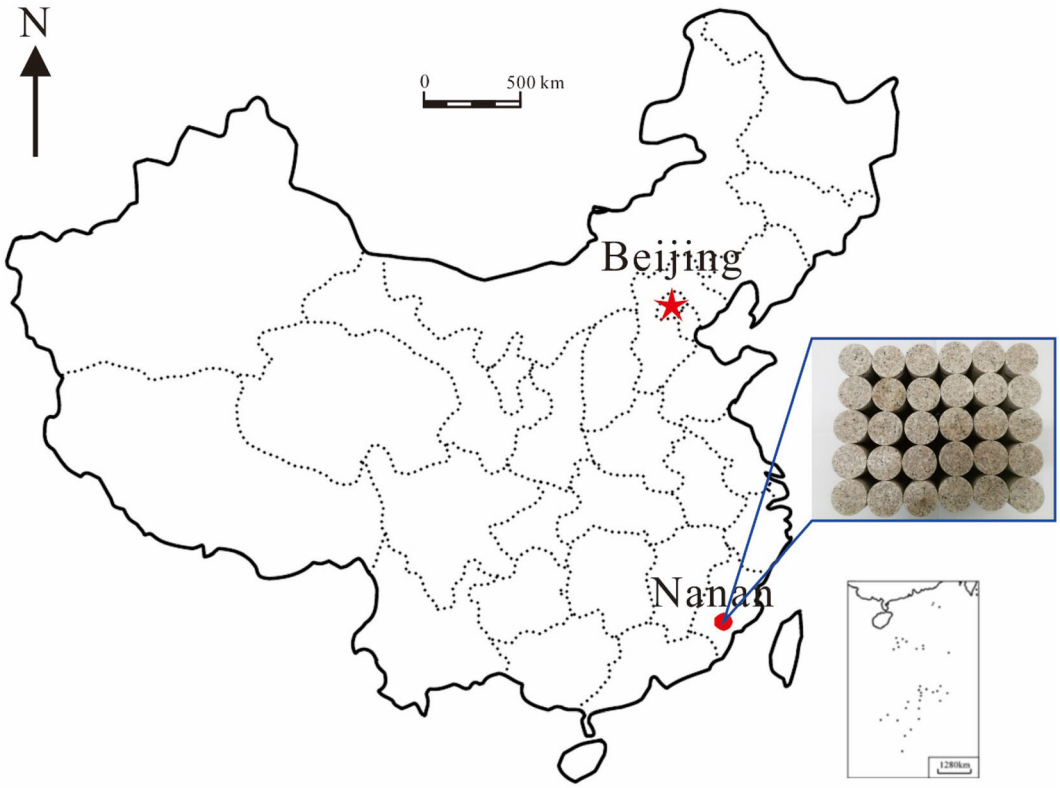


**Figure 1.** Location map for the Nanan granite and untreated granite specimens (the red solid dot is the sampling location).

stress first loaded to the desired value (i.e., 20, 40 and 60 MPa) at a rate of 0.1 MPa/s in the loading triaxial compression tests. For the unloading condition determination, the stress at the starting point of unloading (unloading point) should be higher than UCS and approximately 60–80% of the triaxial compressive strength (Qiu et al. 2014; Huang et al. 2017). Therefore, the confining stress was first loaded to the same desired level as in the loading test, the axial pressure was then loaded at a rate of 0.005 mm/s under axial displacement control until the deviatoric stress was applied to 70% of the corresponding triaxial compressive strength under each confining stress. Finally, the axial stress continued to increase, while the confining stress was gradually unloaded at a rate of 0.05 MPa/s until the specimen failed. During the unloading process, increasing axial stress and decreasing confining pressure were used to simulate the stress variations of the surrounding rock (Li et al. 2017; Meng et al. 2018). The test results are reported in Table 1.

## EXPERIMENTAL RESULTS

### P-wave Velocity

The ultrasonic test has been widely used to detect the interior damage in rock materials (Rong et al. 2018). Therefore, P-wave velocity of granite after high temperature was measured to reflect the evaluation of thermal damage in this study. Thermal damage ($D_p$) is further defined adopting P-wave velocity (Liu and Xu 2015):

$$D_p = 1 - \left(\frac{V_{pT}}{V_{p0}}\right)^2 \tag{1}$$

where $V_{pT}$ is P-wave velocity of granite after high temperature exposure, and $V_{p0}$ is P-wave velocity of granite before thermal treatment.

The relationships between temperature and the P-wave velocity and thermal damage of granite are plotted in Figure 4. The dispersion of P-wave velocity in granite after exposure to high tempera-

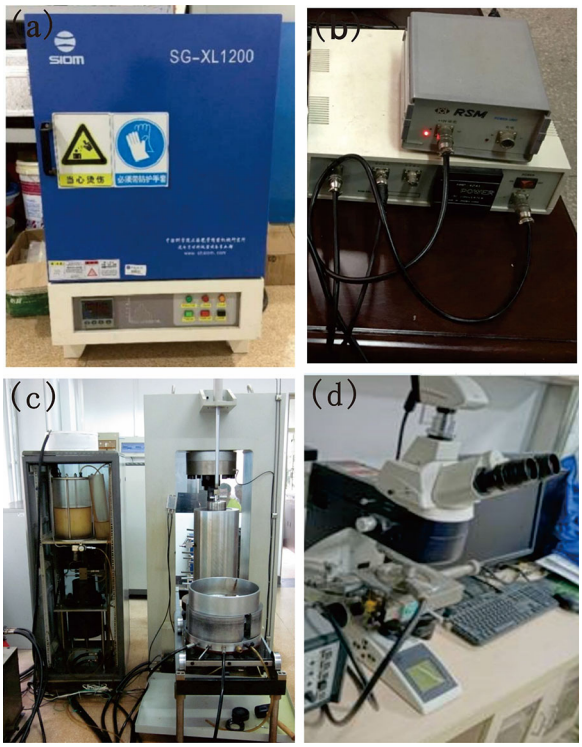


**Figure 2.** Experimental instruments: (**a**) High-temperature box furnace. (**b**) Ultrasonic tester. **c** Servo-controlled compression machine. (**d**) Optical microscope.

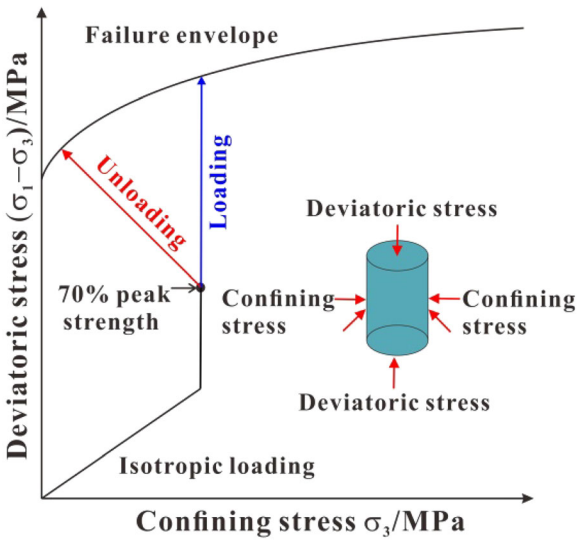


**Figure 3.** Schematic diagram of stress conditions for loading/unloading testing.

tures is very small. The average values of P-wave velocity decrease nearly linearly with increasing temperature. The average value of P-wave velocity decreases to 1077 m/s at 600 °C, which is equivalent to 25.8% of $V_{p0}$, only. Thermal damage shows an opposite trend with increasing temperature, and reached 0.93 at 600 °C, which indicated that the granite specimens had experienced a huge thermal damage at 600 °C.

## Stress–strain Curves

The complete deviatoric stress–strain relations for the granite exposed to various temperatures under loading and unloading conditions are plotted in Figures 5 and 6, respectively. At different high temperatures, the evolution rules of the deviatoric stress with axial, radial and volumetric strains have roughly similar forms under the loading and confining pressure unloading conditions.

The deviatoric stress-axial strain curves under both, loading and unloading conditions were similar and exhibited four stages: compaction, elastic deformation, yield and failure. The initial compaction stage increased as temperature increased from 20 to 600 °C, whereas it decreased clearly with confining stress. In all temperature cases, the deviatoric stress increased linearly with axial strain in the elastic deformation stage, and the yield stage was quite short for the granite specimens under both loading conditions. In the failure stage, the deviatoric stress dropped abruptly at an extremely small axial strain, and the specimens showed evident characteristics of brittle failure.

The radial strain decreased with the applied confining stress under loading conditions, because the existence of the confining stress had an inhibitory effect on the expansion of radial strain. However, after reaching the unloading point, the radial strain was greater than that under loading conditions. The radial strain was more significant near the utmost strength with increasing confining stress, and the specimens exhibited an obvious characteristic of lateral dilatancy. Figure 6 indicates that the point of radial dilation decreased with temperature.

The volumetric strain can be regarded as approximately the sum of the axial strain and twice the radial strain (Chen et al. 2016; Meng et al. 2018). As shown in Figures 5 and 6, the volumetric strains under loading and unloading conditions were both characterized by an initial phase of compaction-dominated behavior followed by a phase of dilatancy-dominated behavior. Compared to conven-

**Table 1.** Physical and mechanical properties of granite after thermal treatments

| Stress condition | Number | $T$ (°C) | $\sigma_3$ (MPa) | $V_p$ (m/s) | $(\sigma_1-\sigma_3)$ (MPa) | $E$ (GPa) | $\varepsilon_s$ (%) | $V$ | $\sigma_{3f}$ (MPa) | $(\sigma_1-\sigma_{3f})$ (MPa) |
|---|---|---|---|---|---|---|---|---|---|---|
| Loading | 1–0–0 | 20* | 0 | 4167 | 163.69 | 24.03 | 0.983 | 0.228 | – | – |
| | 1–1–0 | 200 | 0 | 3571 | 148.05 | 22.12 | 0.949 | 0.227 | – | – |
| | 1–2–0 | 300 | 0 | 3030 | 128.57 | 21.60 | 0.916 | 0.223 | – | – |
| | 1–3–0 | 400 | 0 | 2564 | 130.10 | 21.81 | 0.983 | 0.215 | – | – |
| | 1–4–0 | 500 | 0 | 2000 | 124.02 | 19.14 | 1.030 | 0.216 | – | – |
| | 1–5–0 | 600 | 0 | 1087 | 71.24 | 12.91 | 0.940 | 0.207 | – | – |
| | 1–0–1 | 20* | 20 | 4167 | 252.75 | 24.35 | 1.403 | 0.233 | – | – |
| | 1–1–1 | 200 | 20 | 3571 | 234.44 | 22.74 | 1.408 | 0.232 | – | – |
| | 1–2–1 | 300 | 20 | 2941 | 230.37 | 21.19 | 1.374 | 0.227 | – | – |
| | 1–3–1 | 400 | 20 | 2500 | 223.70 | 21.62 | 1.429 | 0.228 | – | – |
| | 1–4–1 | 500 | 20 | 2000 | 172.61 | 20.26 | 1.209 | 0.223 | – | – |
| | 1–5–1 | 600 | 20 | 1064 | 112.71 | 13.17 | 1.244 | 0.219 | – | – |
| | 1–0–2 | 20* | 40 | 4167 | 294.17 | 24.43 | 1.603 | 0.243 | – | – |
| | 1–1–2 | 200 | 40 | 3571 | 274.87 | 23.20 | 1.654 | 0.238 | – | – |
| | 1–2–2 | 300 | 40 | 3030 | 268.82 | 22.69 | 1.593 | 0.238 | – | – |
| | 1–3–2 | 400 | 40 | 2564 | 269.59 | 21.64 | 1.532 | 0.225 | – | – |
| | 1–4–2 | 500 | 40 | 2000 | 190.49 | 20.51 | 1.306 | 0.227 | – | – |
| | 1–5–2 | 600 | 40 | 1099 | 121.79 | 14.73 | 1.242 | 0.218 | – | – |
| | 1–0–3 | 20* | 60 | 4167 | 355.38 | 26.25 | 1.691 | 0.251 | – | – |
| | 1–1–3 | 200 | 60 | 3571 | 314.45 | 24.40 | 1.741 | 0.246 | – | – |
| | 1–2–3 | 300 | 60 | 2941 | 286.04 | 24.09 | 1.621 | 0.243 | – | – |
| | 1–3–3 | 400 | 60 | 2564 | 278.91 | 24.24 | 1.643 | 0.241 | – | – |
| | 1–4–3 | 500 | 60 | 2041 | 261.50 | 21.58 | 1.610 | 0.242 | – | – |
| | 1–5–3 | 600 | 60 | 1099 | 179.47 | 19.07 | 1.557 | 0.228 | – | – |
| Unloading | 2–0–1 | 20* | 20 | 4167 | 225.93 | 20.76 | 1.386 | 0.24 | 6.20 | 176.92 |
| | 2–1–1 | 200 | 20 | 3571 | 219.34 | 20.68 | 1.365 | 0.24 | 6.20 | 164.11 |
| | 2–2–1 | 300 | 20 | 3030 | 208.94 | 18.46 | 1.340 | 0.24 | 6.60 | 161.26 |
| | 2–3–1 | 400 | 20 | 2564 | 200.96 | 18.43 | 1.262 | 0.23 | 8.30 | 156.59 |
| | 2–4–1 | 500 | 20 | 2128 | 160.91 | 17.31 | 1.236 | 0.22 | 8.40 | 120.82 |
| | 2–5–1 | 600 | 20 | 1064 | 104.27 | 12.41 | 1.243 | 0.22 | 8.80 | 78.90 |
| | 2–0–2 | 20* | 40 | 4167 | 276.13 | 24.39 | 1.480 | 0.246 | 21.02 | 205.92 |
| | 2–1–2 | 200 | 40 | 3571 | 258.15 | 22.94 | 1.480 | 0.246 | 22.01 | 192.41 |
| | 2–2–2 | 300 | 40 | 3030 | 242.92 | 21.64 | 1.482 | 0.238 | 23.60 | 188.17 |
| | 2–3–2 | 400 | 40 | 2564 | 238.00 | 21.62 | 1.404 | 0.236 | 25.20 | 188.71 |
| | 2–4–2 | 500 | 40 | 2041 | 173.44 | 19.07 | 1.418 | 0.234 | 26.40 | 133.34 |
| | 2–5–2 | 600 | 40 | 1042 | 112.96 | 13.43 | 1.346 | 0.228 | 28.00 | 85.26 |
| | 2–0–3 | 20* | 60 | 4167 | 327.03 | 25.24 | 1.597 | 0.255 | 38.50 | 248.76 |
| | 2–1–3 | 200 | 60 | 3571 | 294.92 | 24.34 | 1.593 | 0.253 | 38.52 | 220.11 |
| | 2–2–3 | 300 | 60 | 3030 | 257.48 | 22.52 | 1.537 | 0.247 | 38.65 | 200.23 |
| | 2–3–3 | 400 | 60 | 2564 | 253.76 | 22.08 | 1.529 | 0.245 | 39.00 | 195.24 |
| | 2–4–3 | 500 | 60 | 2041 | 241.37 | 20.89 | 1.511 | 0.244 | 42.59 | 183.05 |
| | 2–5–3 | 600 | 60 | 1087 | 164.04 | 18.82 | 1.305 | 0.238 | 43.00 | 125.63 |

* is expressed as room temperature. $\sigma_{3f}$ is the confining stress of rock remaining at failure. $\varepsilon_s$ is the peak stain at failure

tional triaxial compression, the peak volumetric strain under unloading conditions was more significant. After reaching the unloading point, the volumetric strain dilated gradually with decreasing confining stress, and it became more significant near the critical point of failure. The dilation of the volumetric strain also increased with the initial confining stress. High temperature had a great effect on the expansion of the volumetric strain: the higher the temperature, the more easily volumetric dilation occurred.

## Strength and Deformation Characteristics

The variations in the peak deviatoric stress ($\sigma_1-\sigma_3$), elastic modulus ($E$) and Poisson's ratio ($v$) of the treated granite under loading and unloading conditions are shown in Figure 7. The results show that the peak strengths during loading and unloading decreased as temperature increased, with the trend becoming more obvious as temperature continued to increase to 400 °C. At 600 °C, the peak strengths decreased by 55.4%, 58.6%, and 49.5% under con-

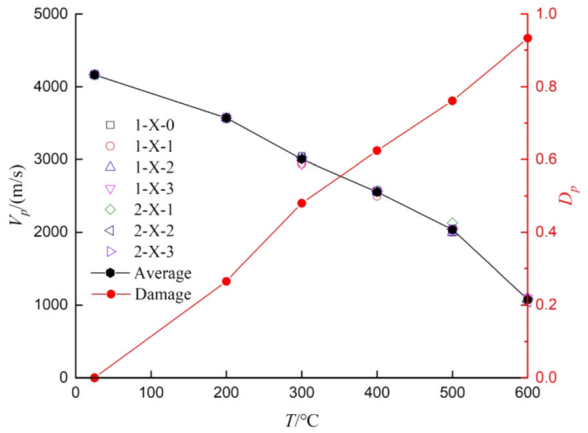


**Figure 4.** Relationships between temperature, the P-wave velocity and thermal damage of granite.

fining pressures of 20, 40 and 60 MPa, respectively, while these values became 53.9%, 59.1% and 49.8% for unloading conditions. Figure 7a shows that the peak strengths under unloading conditions decreased by 8.34% compared with values obtained in conventional triaxial compression tests. Therefore, both unloading and thermal treatment decrease the carrying capacity of granite specimens. However, there were some differences in the deterioration mechanism, which will be described in detail in the next section.

As shown in Figure 7b, the unloading condition decreased the elastic modulus of the specimens exposed to various treatment temperatures from the perspective of different loading conditions. However, the elastic modulus increased with confining stress, not only under loading conditions, but also under unloading conditions. $E$ decreased minimally with temperature, and subsequently decreased sharply after thermal heating to 400 °C. With further increase in temperature to 600 °C, $E$ decreased rapidly by 45.9%, 39.7%, and 33.5% under loading conditions with confining stresses of 20, 40 and 60 MPa, respectively, with values of 40.2%, 44.9% and 25.4% for unloading conditions, which also indicated a decrease in the carrying capacity of the granite specimens.

Figure 7c shows the effect of temperature on the Poisson's ratio of granite under two loading conditions. The increase in the Poisson's ratio of the specimens after their thermal treatments from the loading to the unloading condition indicated an expansion of the radial strain. At the same time, the values of the Poisson's ratio decreased slightly with temperature.

## Failure Criterion

The Mohr–Coulomb (MC) (Labuz and Zang 2012) and Hoek–Brown (HB) (Hoek and Brown 1980) failure criteria are both suitable for evaluating the damage of rocks and are expressed by the following equations, respectively:

$$\sigma_1 = \frac{1+\sin\varphi}{1-\sin\varphi}\sigma_3 + \frac{2c\cos\varphi}{1-\sin\varphi} \tag{2}$$

$$\sigma_1 = \sigma_3 + \sigma_{ci}\sqrt{m_i\frac{\sigma_3}{\sigma_{ci}} + s} \tag{3}$$

where $\sigma_1$ and $\sigma_3$ are maximum and minimum principal stresses, respectively; $c$ and $\varphi$ are cohesion and internal friction angle, respectively; $\sigma_{ci}$ is uniaxial compressive strength of intact rock; and $m_i$ and $s$ are rock mass material constants, respectively, and $s = 1$ for intact rock in this study.

The fitting relationships between peak axial and confining stresses of granite after high temperature treatments, based on the MC and the HB criteria are plotted in Figures 8 and 9, respectively, and the details of the strength and failure parameters are presented in Table 2. As Figures 8 and 9 indicate, the fitting lines based on the two failure criteria had a good agreement with the experimental data. All the coefficients of determination ($R^2$) of these regression lines in Figures 8 and 9 were above 0.931, what indicated that the MC and the HB criteria well reflect the failure characteristics of granite after exposure to temperatures under both, loading and unloading conditions. Compared to the MC criterion, the HB criterion had larger coefficients of determination ($R^2$) of these regression lines in general and it was more suitable for evaluating the damage of granite after thermal treatment under loading and unloading conditions.

The temperature-dependent characteristics of $c$ and $\varphi$, $\sigma_{ci}$ and $m_i$ of the investigated granite are shown in Figures 10 and 11. Cohesion and friction angle both decreased with increasing temperature under the two loading approaches. The cohesion under unloading conditions was larger than that under loading conditions, while the internal friction angle exhibited a different trend. The values of cohesion under the loading conditions decreased by

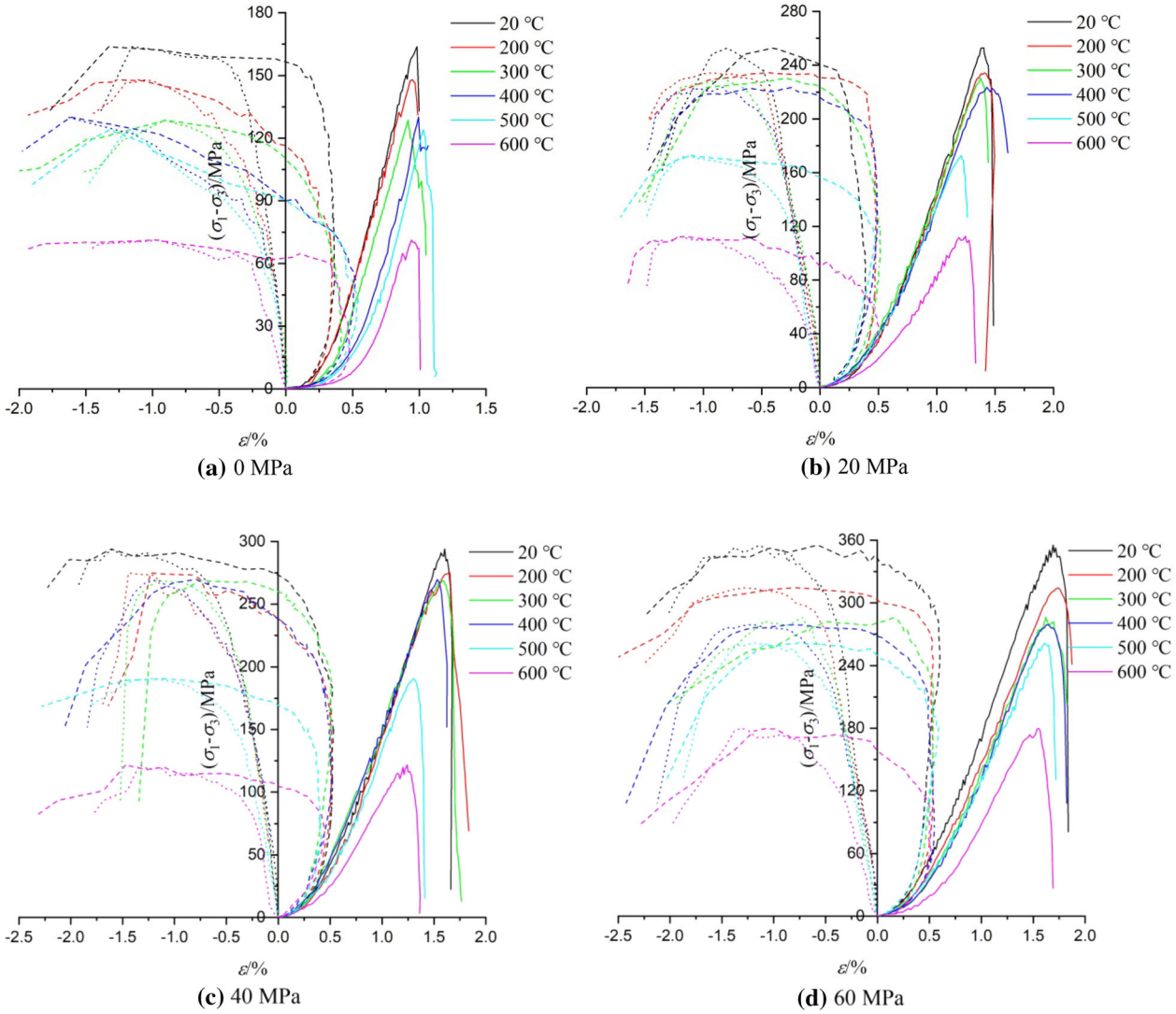


**Figure 5.** Integrated stress–strain curves of granite at temperatures under loading condition (solid lines represent axial strain; dotted lines represent radial strain; dashed lines represent volumetric strain).

5.3%, 19.8% and 49.4% at 400, 500 and 600 °C, respectively, compared with the values at room temperature, and the values under the unloading condition decreased to 4.5%, 9.2% and 33.5% at these temperatures, respectively. The internal friction angle under loading conditions decreased by 10.3%, 16.4% and 27.5% when the temperature increased to 400, 500 and 600 °C, respectively. The values of $\sigma_{ci}$ and $m_i$ decreased with increasing temperature under the loading and unloading conditions, and the values of $\sigma_{ci}$ and $m_i$ under unloading conditions were larger than those under loading conditions.

## DISCUSSION

### Effects of High Temperatures on Mechanical Behaviors

As shown in Figures 6 and 7, the peak strength, elastic modulus, Poisson's ratio, cohesion and internal friction angle under both, loading and unloading conditions, decreased with increasing temperature. This means that thermal treatment reduces the carrying capacity of the investigated granite specimens. Under both loading stress approaches, the peak strength, elastic modulus, cohesion and internal

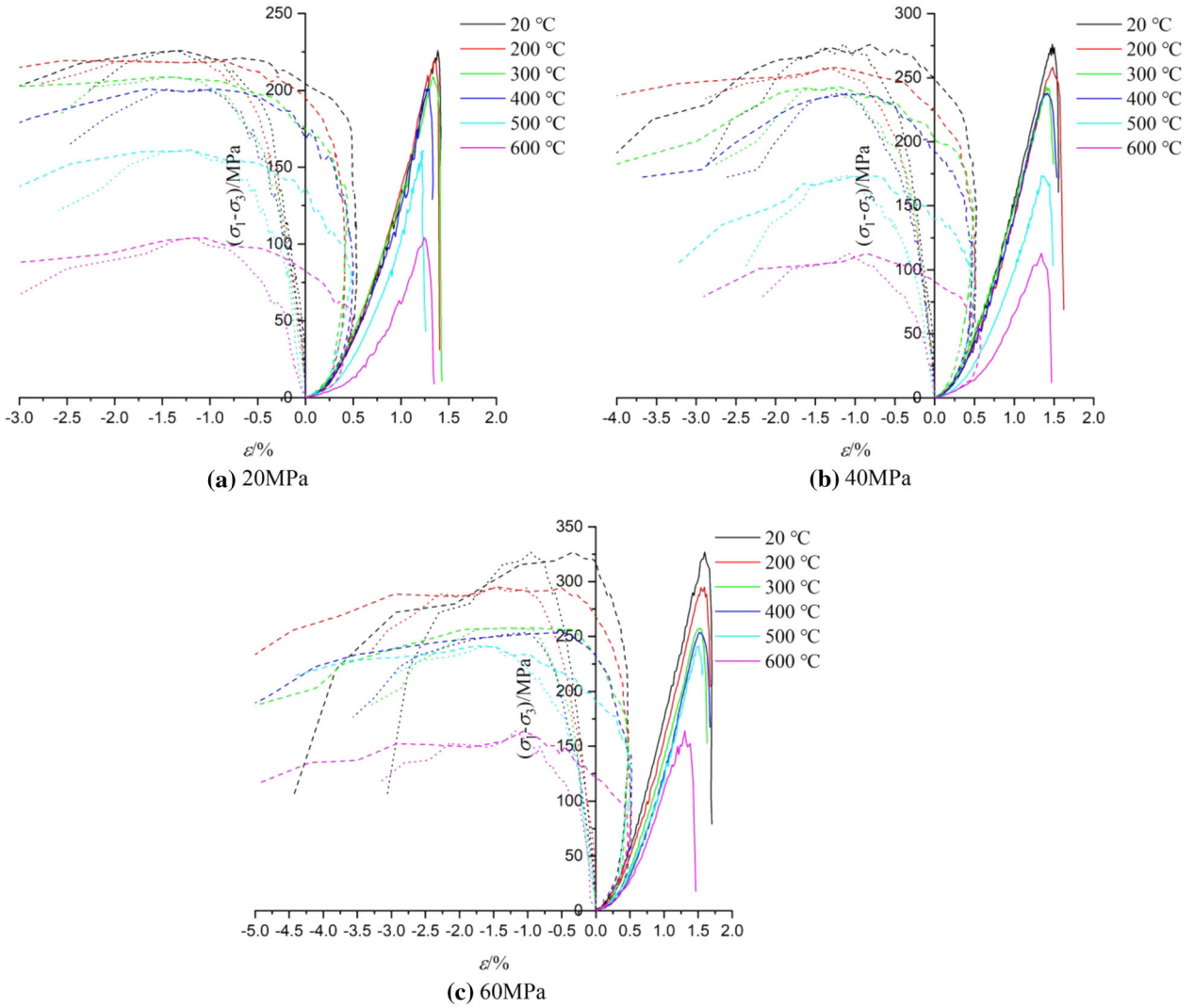


**Figure 6.** Integrated stress–strain curves of granite at temperatures under unloading condition (solid lines represent axial strain; dotted lines represent radial strain; dashed lines represent volumetric strain).

friction angle initially decreased slowly up to temperatures of 400 °C, and rapidly above these. It appears that 400 °C can be considered as a threshold temperature for the present granite samples. Figures 5 and 6 indicate that the higher the temperature, the more radial and volumetric dilation occur, which demonstrates that high temperatures have a great influence on the mechanical properties of granite. Many studies have shown that observed variations in mechanical properties are related to changes in the rock microstructure after thermal treatment (Fan et al. 2018; Rong et al. 2018; Han et al. 2019; Wu et al. 2019a).

The microscopic change mechanism of the mechanical behaviors of granite after thermal treatment was revealed by optical microscopy analysis. For that purpose, it was enlarged 200 times with the results presented in Figure 12. As Figure 12a indicates, some micro-cracks can be found, while the grains were well arrayed at room temperature in general. With increasing temperature, mineral thermal expansion resulted in notable effects on the rock micro-structure. After a thermal treatment up to 200 °C, grain boundary micro-cracks began to propagate between different minerals (Fig. 12b). At 300 °C, intra-granular micro-cracks can be observed, not

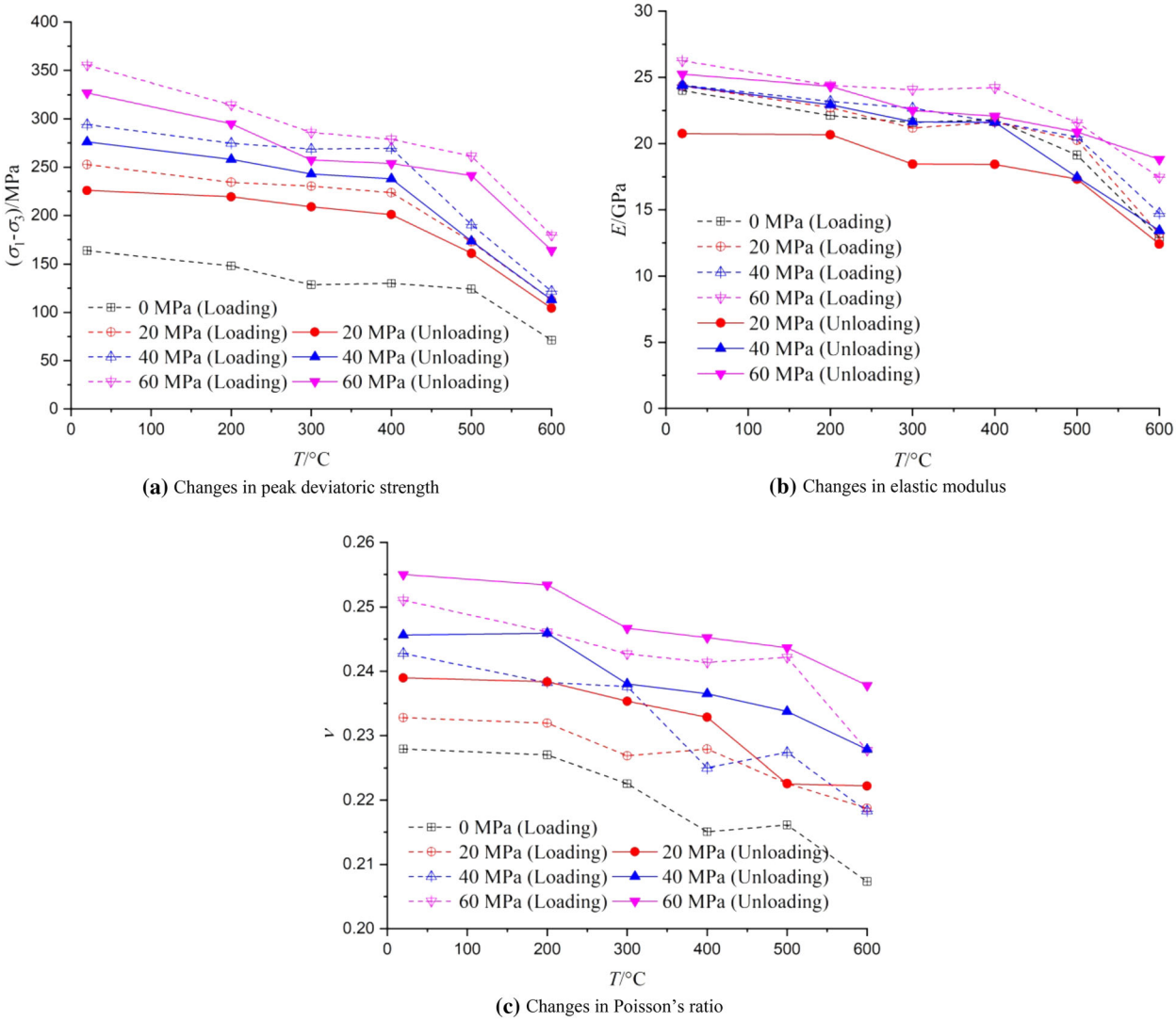


**(a)** Changes in peak deviatoric strength

**(b)** Changes in elastic modulus

**(c)** Changes in Poisson's ratio

**Figure 7.** Changes in peak deviatoric strength ($\sigma_1$–$\sigma_3$), elastic modulus ($E$) and Poisson's radio ($v$) of granite after thermal treatment under loading (dashed lines) and unloading conditions (solid lines).

only in the feldspar grains, but also in the quartz grains. With further increase in temperature up to 400 °C, more grain boundary and intra-granular micro-cracks were observed in the granite specimens. When the temperature was increased to 500 °C, the micro-crack density and width increased, and a micro-crack network was formed in parts of the thin sections. The increased pressure due to the liquid to gaseous phase transition of water could also induce micro-cracks in granite. Many thermal micro-cracks in the specimen heated to 600 °C were further extended and coalesced.

Thermal treatment induces expansion of mineral grains and changes in the mineral composition (Somerton 1993; Glover et al. 1995; Zhang et al. 2016). As a result, micro-cracks initiate and propagate along different mineral grains or inside the same mineral grains, which causes decreases in the peak strength, elastic modulus, Poisson's ratio, cohesion, and friction angle of the granite specimens under both loading and unloading conditions. As presented in Figure 12, the formation of a micro-crack network was observed in the thin sections after treatment at 400 °C. This resulted in a more rapid decrease in the strength and deformation charac-

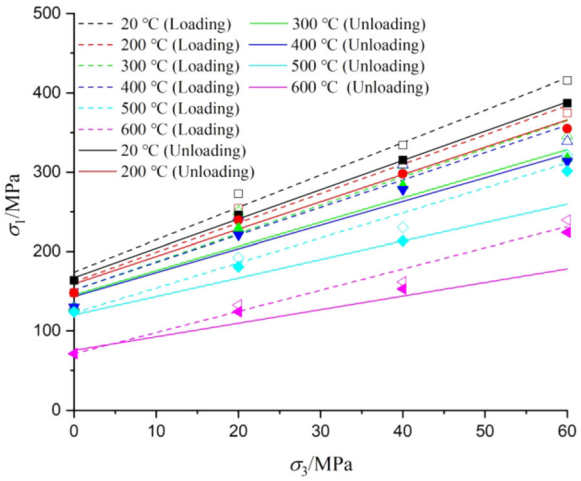


**Figure 8.** Fitting relationship between peak axial and confining stresses of granite after high temperature treatments based on the MC criterion.

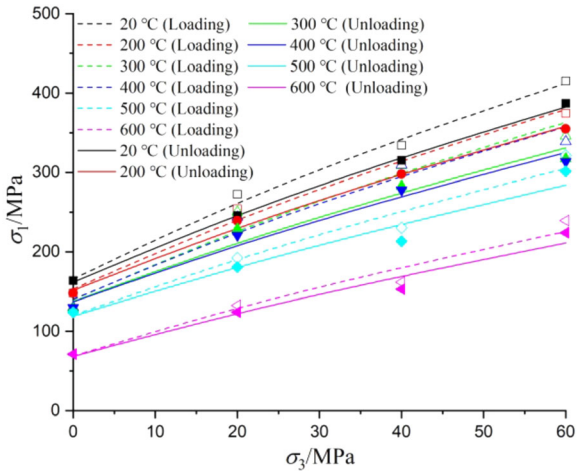


**Figure 9.** Fitting relationship between peak axial and confining stresses of granite after high temperature treatments based on the HB criterion.

teristics under loading and unloading conditions. With increase in temperature, an increasing number of grain boundary and intra-granular micro-cracks were induced, while the lateral tensile stress more easily induced the extension of tension cracks parallel to the axial direction (Meng et al. 2018). Therefore, the higher the temperature, the more easily radial and volumetric dilation occur under unloading conditions.

In order to quantify the propagation of micro-cracks of granite against elevated temperature, micro-crack density ($\rho_f$) (Nasseri et al. 2007) and average width ($W_a$) were introduced as follows:

$$\rho_f = \frac{L_c}{S} \tag{4}$$

$$W_a = \frac{S_c}{L_c} \tag{5}$$

where $L_c$ is total length of micro-cracks sketched and calculated in the thin section of granite after high temperature treatment using the ImageJ software package (Schindelin et al. 2012); $S$ and $S_c$ are the calculated total and micro-crack area of a granite thin section, respectively. It should be noted that the width of micro-cracks was ignored in the micro-crack density calculation for granite after high temperature treatment.

Relationships between temperature and micro-crack density as well as average width of granite after high temperature exposure are shown in Table 2 and Figure 13. As Figure 13 indicates, both $\rho_f$ and $W_a$ of the micro-cracks increased with increasing temperature, which is consistent with the deterioration of mechanical properties (Figure 7). At 600 °C, the micro-crack density and average width of granite reached 3.64 mm/mm$^2$ and 11.50 μm, respectively.

## Effects of Loading and Unloading on Mechanical Behaviors

Unloading stress conditions have a significant influence on mechanical characteristics of rocks. First, based on a comparison of Figures 5 and 6, the radial and volumetric strains increased more under unloading conditions, which meant that the unloading process induces greater radial dilation in the granite specimens. Second, as shown in Figure 7, the peak deviatoric stress and elastic modulus under unloading conditions were 8.34% and 7.31% lower than those obtained in conventional triaxial tests, which indicated that the unloading approach also reduces the carrying capacity of granite specimens.

Poisson's ratio is computed as the negative ratio of the radial to axial strain, and its value reflects changes in radial strain during unloading (Meng et al. 2018). To describe the changes in the Poisson's ratio during unloading, the unloading ratio ($H$) is introduced to characterize its degree, which is defined as:

$$H = \frac{\left|\sigma_3^T - \sigma_3^0\right|}{\sigma_3^0} \tag{6}$$

**Table 2.** Strength and failure parameters of granite after high temperature treatments under triaxial compression

| Stress condition | $T$ (°C) | Mohr–Coulomb criterion | | | Hoek–Brown criterion | | | $\rho f$ (mm/mm$^2$) | $Wa$ (μm) |
|---|---|---|---|---|---|---|---|---|---|
| | | $\varphi$(°) | $C$(MPa) | $R^2$ | $m_i$ | $\sigma_{ci}$( MPa) | $R^2$ | | |
| Loading | 20 | 37.34 | 43.08 | 0.988 | 165.82 | 9.72 | 0.995 | 0.80 | 2.24 |
| | 200 | 35.05 | 42.14 | 0.977 | 153.23 | 8.55 | 0.993 | 1.40 | 4.63 |
| | 300 | 34.11 | 40.28 | 0.931 | 139.68 | 8.63 | 0.966 | 1.84 | 6.67 |
| | 400 | 33.49 | 40.79 | 0.931 | 140.34 | 8.18 | 0.965 | 2.01 | 7.21 |
| | 500 | 31.22 | 34.54 | 0.977 | 120.15 | 6.34 | 0.964 | 2.55 | 8.76 |
| | 600 | 27.07 | 21.80 | 0.973 | 68.89 | 5.48 | 0.961 | 3.64 | 11.50 |
| Unloading | 20 | 35.04 | 43.46 | 0.999 | 161.73 | 8.03 | 0.998 | – | – |
| | 200 | 33.03 | 42.93 | 0.985 | 151.50 | 7.25 | 0.997 | – | – |
| | 300 | 30.84 | 41.56 | 0.945 | 137.81 | 6.59 | 0.971 | – | – |
| | 400 | 30.33 | 41.45 | 0.960 | 137.12 | 6.25 | 0.981 | – | – |
| | 500 | 28.48 | 35.80 | 0.966 | 119.09 | 5.04 | 0.951 | – | – |
| | 600 | 24.70 | 22.45 | 0.975 | 68.53 | 4.42 | 0.963 | – | – |

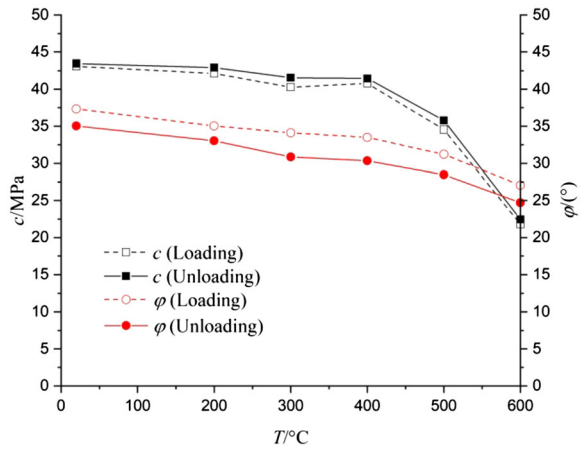


**Figure 10.** Cohesion and friction angle as functions of temperature under loading and unloading conditions.

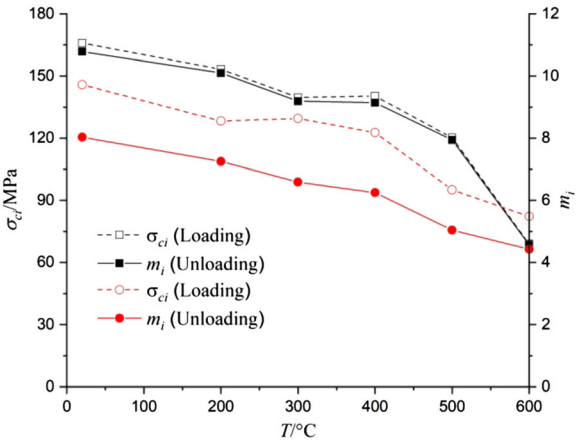


**Figure 11.** $\sigma_{ci}$ and $m_i$ as functions of temperature under loading and unloading conditions.

where $H$ is unloading ratio, $\sigma_3^0$ is initial confining stress, and $\sigma_3^T$ is confining stress during the unloading process.

Figure 14 reveals that there was an exponential relationship between the Poisson's ratio and the unloading ratio of granite after exposure to high temperatures. The Poisson's ratio increased slowly at the beginning of the unloading process and then increased rapidly near the unloading failure. During the unloading process, the Poisson's ratio exceeded 0.5 (the Poisson's ratio limit of elastoplastic materials). Unloading conditions caused a high increase in radial deformation, which included not only rock elastic deformation, but also crack propagation. The deformation caused by the propagation of cracks was far larger than the elastic deformation. According to the definition of Poisson's ratio, the rapid increase in radial strain under unloading conditions will cause the sharp increase in Poisson's ratio. As a result, the Poisson's ratio of granite under the unloading condition was bigger than 0.5.

To present the expansion in radial deformation during the loading process more clearly, the relationships between the axial, radial and volumetric strains and confining stress are plotted in Figure 15. The axial strain increased very slowly, while the radial strain expanded rapidly with the confining stress, especially near the failure point. The value of expansion in the radial strain was 4 to 6 times greater than that in the axial strain of granite exposed to elevated temperatures. The volumetric strain is the sum of the axial strain and twice the

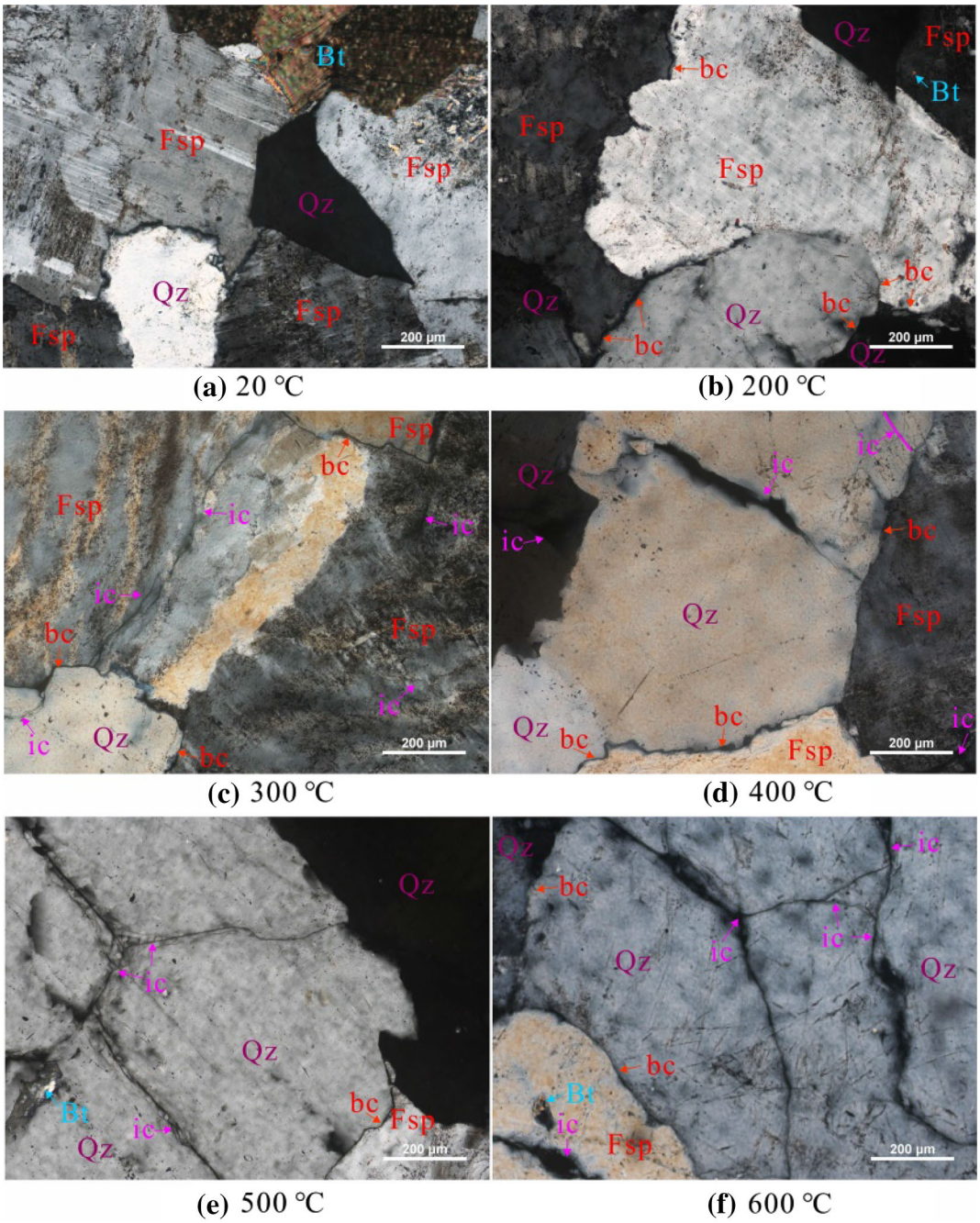


**Figure 12.** Optical microscopic images of granite after treatment at temperatures up to 600 °C (''Qz'' represents quartz; ''Fsp'' represents feldspar; ''Bt'' represents biotite; ''bc'' means ''grain boundary micro-crack''; ''ic'' means ''intra-granular micro-crack'').

radial strain, exhibiting a similar trend to the radial strain during unloading. The relationships between the volumetric strain and axial strain of granite after exposure to elevated temperatures under the two loading conditions are shown in Figure 16. The volumetric strain under unloading conditions expanded more dramatically, and the maximum value of expansion in volumetric strain under unloading (Fig. 16b) was twice that under loading conditions (refer to Fig. 16a).

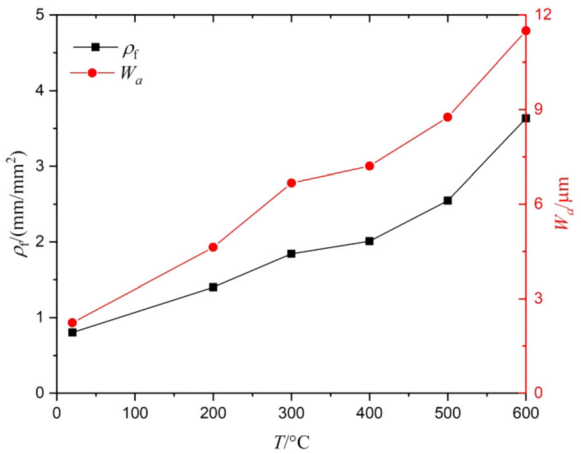


**Figure 13.** Relationships between temperature, micro-crack density and average width of granite after high temperature treatment.

The difference between the two loading stress conditions in this study is that the confining stress was unloaded gradually under unloading conditions. In essence, the unloading stress state is equivalent to superimposing a lateral tensile stress on the loading stress state. This lateral tensile stress induces the extension of tension cracks parallel to the axial direction, and tension cracks gradually develop in the interior of rock specimens with increasing lateral tensile stress (Dai et al. 2018). As a result, the specimen exhibited radial dilation under unloading conditions. The tension cracks induced by the lateral tensile stress extended gradually and coalesced with decreasing confining stress, which caused deterioration of the peak strength under the loading approach. Therefore, the rock specimens were more likely to be destroyed, and the carrying capacity of granite specimens decreased.

## Combined Effect of Thermal Treatment and Loading Stress Conditions on Mechanical Behaviors

As demonstrated in the present study, both high-temperature and unloading treatments degraded the mechanical properties and decreased the carrying capacity of granite, although their deterio-

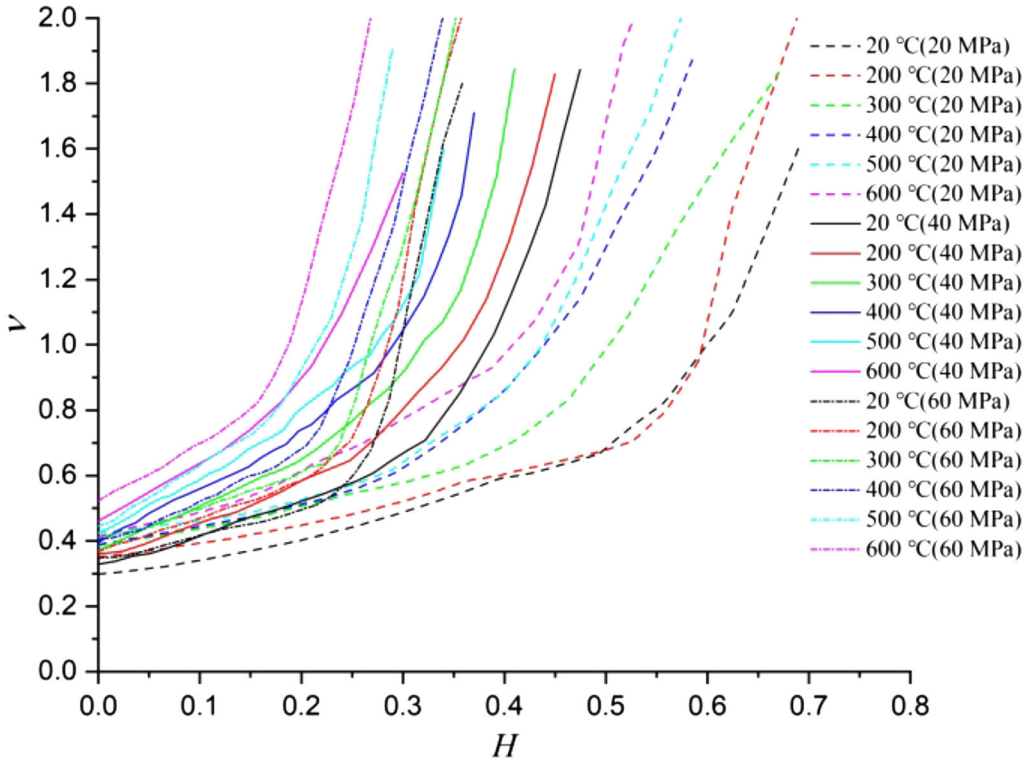


**Figure 14.** Relationships between Poisson's ratio and unloading ratio at various temperatures and confining stresses.

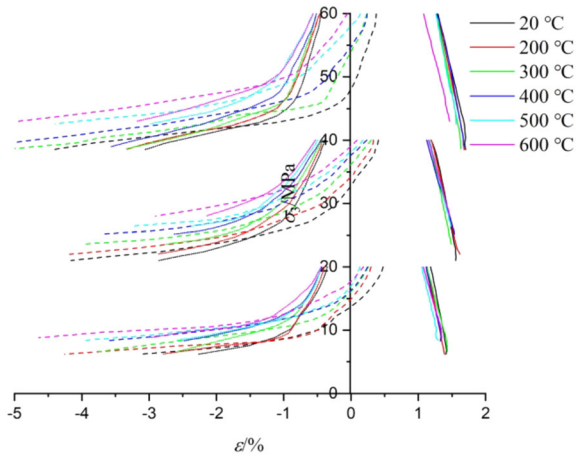


**Figure 15.** Relationships between axial, radial and volumetric strains and confining pressure during loading (solid lines represent axial strain; dotted lines represent radial strain; dashed lines represent volumetric strain).

ration mechanisms were not identical. The changes in strength and deformation characteristics reflect rock damage, and the use of methods of damage mechanics to study temperature-dependent rock behaviors is an innovative approach in rock mechanics (Liu and Xu 2015). A thermal damage variable ($D_T$) was introduced to quantify the degree of damage to granite after high-temperature treatment and defined as:

$$D_T = 1 - \frac{I_T}{I_0} \tag{7}$$

where $I_T$ and $I_0$ represent the peak strength, elastic modulus or Poisson's ratio of granite before and after heating treatment, respectively.

To quantify the degree of damage to granite after the unloading treatment, an unloading damage variable ($D_U$) was similarly defined to $D_T$ as:

$$D_U = 1 - \frac{K_U}{K_0} \tag{8}$$

where $K_T$ and $K_0$ represent the peak strength, elastic modulus or Poisson's ratio of granite before and after unloading treatment, respectively.

According to the experimental results presented above, the relationships between temperature and $D_T$ as well as temperature and $D_U$ are presented in Figures 17 and 18, respectively. $D_T$ increased with temperature, and the growth rates of $D_T$, based on the peak strength and elastic modulus, were greater than those based on the Poisson's ratio. $D_T$ increased rapidly at temperatures above 400 °C, which corresponded to the optical microscopy analysis results, where more micro-cracks were observed above 400 °C. $D_U$ decreased with confining stress in general, and $D_U$ on the basis of the Poisson's ratio was less than zero, because the Poisson's ratio of granite under loading conditions was less than that under unloading conditions. In view of Figures 17 and 18, the values of $D_T$, based on peak strength and elastic modulus, exceeded 0.15 above 400 °C, while the values of $D_U$ were less than 0.15 at any confining stress. Further, all values of $D_T$ on the basis of the Poisson's ratio exceeded 0.05 above 400 °C, while the values of $D_T$ were less than 0.05 at any confining stress. Therefore, on the basis of the three mechanical and deformation properties, $D_T$ was greater than $D_U$ after thermal heating to at least 500 °C under any confining stress. In other words, treatment at temperatures above 400 °C had a greater influence on the mechanical characteristics of granite than any unloading treatment, whereby 400 °C can be considered as threshold temperature for significant deterioration in granite properties.

## Potential Applications in Deep Geological Subsurface Utilization

In general, both high-temperature and unloading treatments degrade the mechanical properties and decrease the carrying capacity of granite. On the one hand, during drilling and excavation, the deterioration of strength and elastic behaviors may induce instability of rock surrounding a wellbore or tunnel. Because unloading can lead to a pervasive tensile micro-cracking process before the emergence of macroscopic failure (Dai et al. 2018), it will eventually induce tensile failure accompanied by wall rock breakouts (Siratovich et al. 2016). Meanwhile, the high temperature can result in a microcrack network close to the deep wellbore due to thermally induced cracks (Kumari et al. 2019). The present experimental results illustrated the influence of high-temperature and unloading treatments on the mechanical characteristics, which provide an important basis for the parametrization of analytical and numerical models for the utilization of the geological subsurface. On the other hand, heat extraction in HDR projects entails hydraulic stimulation to establish the required permeability and form an artificial fracture network, connecting the injection well with the production wells across a heater exchanger (Frash et al. 2015). During the

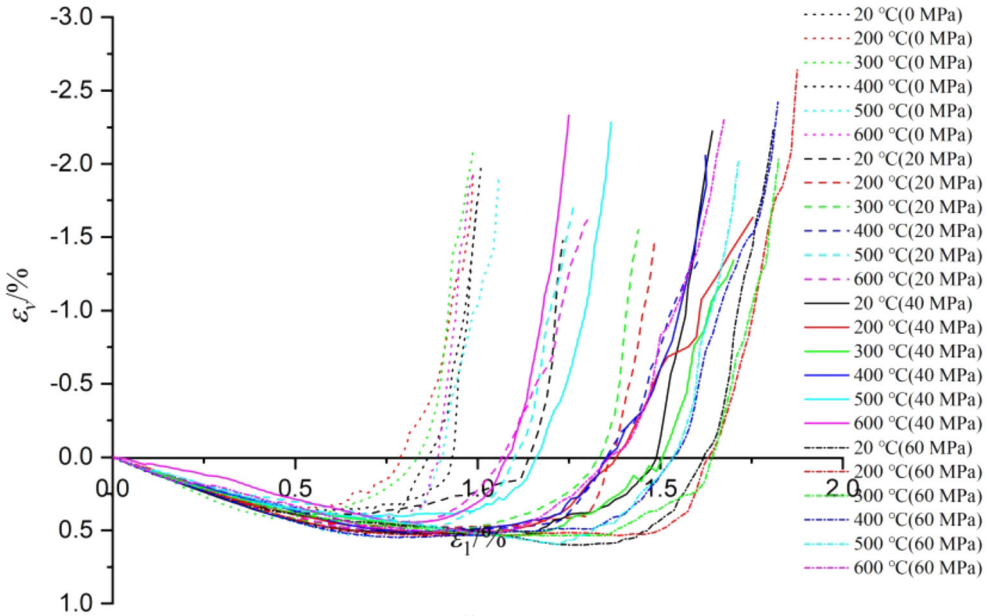


**(a)** Loading condition

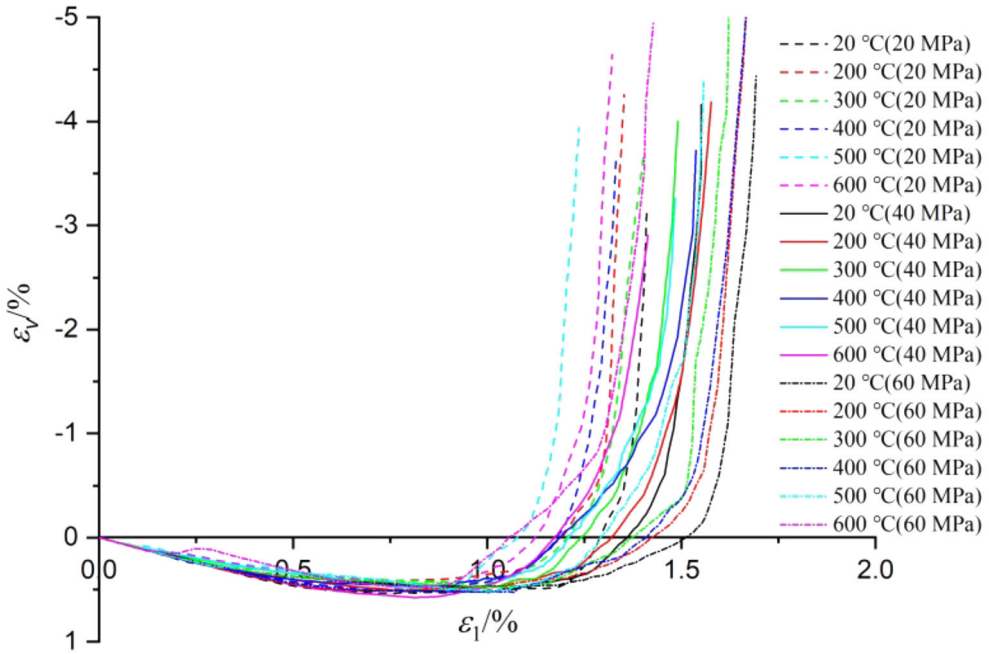


**(b)** Unloading condition

**Figure 16.** Volumetric strain-axial strain curves of granite exposed to various temperatures under loading and unloading conditions.

process of hydraulic fracturing, the breakdown pressure decreases linearly with temperature (Zhang et al. 2019). Considering the degradation of mechanical strength and elastic behaviors of granite in a geothermal reservoir, it will be conducive to well drilling and the stimulation of fracture networks

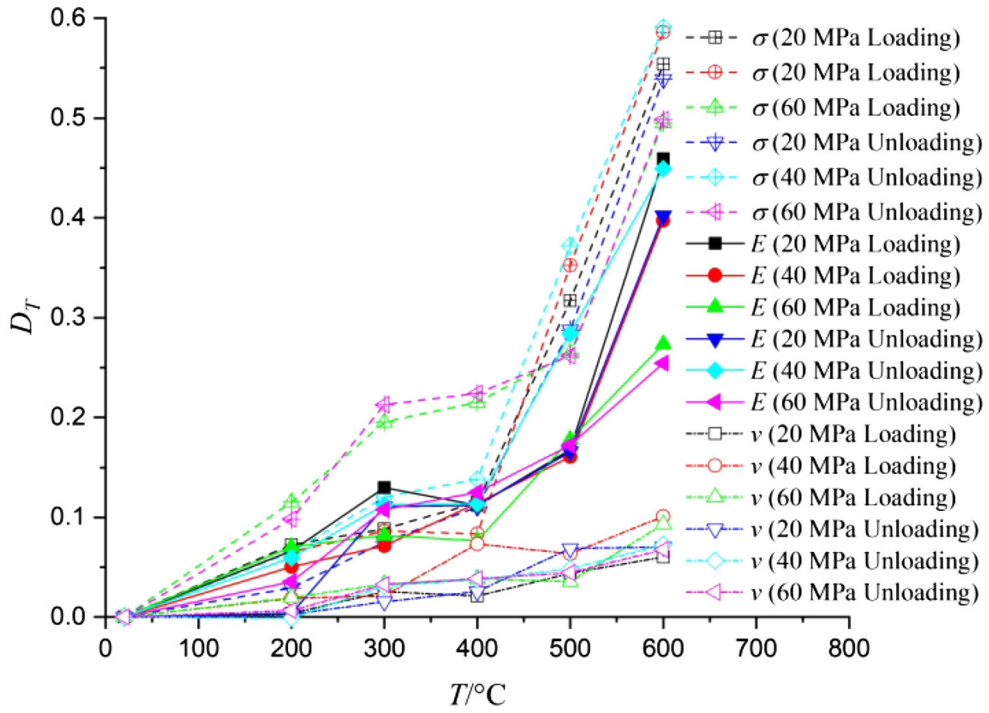


**Figure 17.** Relationship between temperature and thermal damage at various confining stresses.

in HDR reservoirs. Thus, this study will support analytical and numerical modeling of granite exposed to high temperatures during the development of the deep geological subsurface for geothermal energy extraction from hot dry rocks in the Gonghe Basin, China, in the near future.

## CONCLUSIONS

In the present study, a series of loading and unloading triaxial compression tests at 20, 40 and 60 MPa for granite specimens after exposure to elevated temperatures of 200, 300, 400, 500 and 600 °C was carried out to investigate the combined effects of thermal treatment and loading and loading stress conditions on granite strength and deformation. The following conclusions are drawn from the experimental results.

1. Thermal treatment induces deterioration of the strength and deformation properties and decreases the carrying capacity of granite specimens under both loading and unloading conditions. Under loading conditions with an initial confining stress of 60 MPa, the peak strengths decrease by 22.4%, 26.2% and 49.8% at 400, 500 and 600 °C, respectively, compared to the values at room temperature, while the values of the elastic modulus decrease by 12.5%, 17.2% and 25.4%, where temperature increases to 400, 500 and 600 °C, respectively. The values of cohesion under unloading conditions decrease by 4.5%, 9.2% and 33.5% at 400, 500 and 600 °C, respectively, compared to the values at room temperature, whereby the internal friction angle decreases by 14.6%, 33.0% and 56.6% at 400, 500 and 600 °C, respectively.
2. The peak strength and elastic modulus under unloading conditions are reduced, compared with the results obtained from conventional triaxial tests. This indicates that unloading also decreases the carrying capacity of granite. At 600 °C, the peak strengths decrease by 55.4%, 58.6% and 49.5% under confining pressures of 20, 40 and 60 MPa, respectively, while these values are 53.9%, 59.1% and 49.8% under unloading conditions. The elastic modulus decreases rapidly

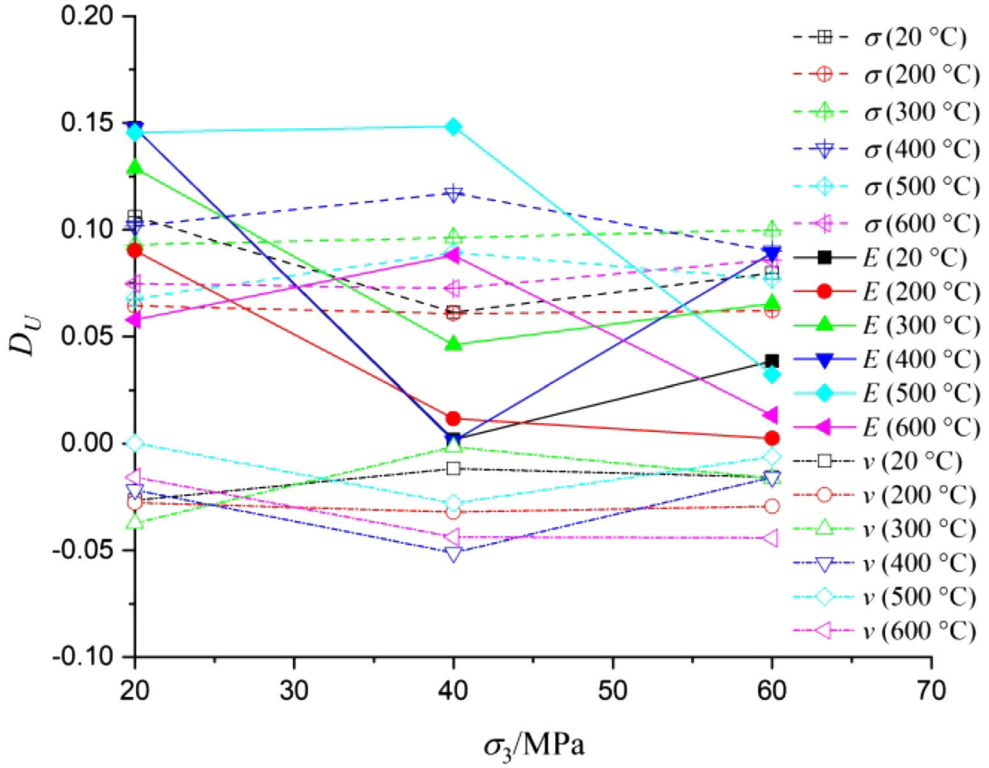


**Figure 18.** Relationship between temperature and unloading damage at various temperatures.

by 45.9%, 39.7% and 27.3% under loading conditions at confining stresses of 20, 40 and 60 MPa, respectively. These values become 40.2%, 44.9% and 25.4% for the unloading path. The cohesion under unloading conditions is greater than that obtained in conventional tests, while the internal friction angle exhibits the opposite trend.

3. The deterioration mechanisms of high-temperature and unloading treatments are not identical. The gradual degradation of the mechanical characteristics of granite after thermal treatment is mainly associated with the evolution of thermal micro-cracks, observed by optical microscopy. High temperatures induce, widen and extend the grain boundary and intra-granular micro-cracks beside or inside mineral grains. The unloading stress state is equivalent to superimposing a lateral tensile stress on the loading stress state. This lateral tensile stress induces the extension of tension cracks parallel to the axial direction and degrades the mechanical characteristics of the granite.
4. $D_T$ and $D_U$ are introduced to compare the effects of high-temperature and unloading treatments on the mechanical characteristics of granite. On the basis of three mechanical and deformation properties, $D_T$ is greater than $D_U$ after thermal heating to 500 °C under any confining stress. 400 °C can be treated as the threshold temperature for significant deterioration, and temperatures above 400 °C have a greater effect on the strength and deformation properties of granite than unloading treatment.
5. The findings of the present study support the parametrization of analytical and numerical models for the assessment of high-temperature drilling and excavation operations in granite.

## ACKNOWLEDGMENTS

This work is jointly supported by National Natural Science Foundation of China (No. 41602374 and No. 41674180), the Fundamental Research Funds for the Central Universities-Cradle Plan for 2017 (Grant No. CUGL170207) and the National Key Research and Development Program of China (No. 2019YFB1504201, No. 2019YFB1504203 and No. 2019YFB1504204).

## REFERENCES

Breede, K., Dzebisashvili, K., Liu, X. L., & Falcone, G. (2013). A systematic review of enhanced (or engineered) geothermal systems: past, present and future. *Geothermal Energy, 1*(1), 4.

Chen, G. Q., Li, T. B., Li, G. M., Qin, C. A., & He, Y. H. (2018). Influence of temperature on the brittle failure of granite in deep tunnels determined from triaxial unloading tests. *European Journal of Environmental and Civil Engineering, 22*(sup1), 269–285.

Chen, J., Jiang, D. Y., Ren, S., & Yang, C. H. (2016). Comparison of the characteristics of rock salt exposed to loading and unloading of confining pressures. *Acta Geotechnica, 11*(1), 221–230.

Clark, S. P. (1966). Handbook of physical constants. *Geological Society of America, 97,* 459–482.

Dai, B., Zhao, G. Y., Konietzky, H., & Wasantha, P. L. P. (2018). Experimental and numerical study on the damage evolution behaviour of granitic rock during loading and unloading. *KSCE Journal of Civil Engineering, 22*(9), 3278–3291.

Ding, Q. L., Ju, F., Mao, X. B., Ma, D., Yu, B. Y., & Song, S. B. (2016). Experimental investigation of the mechanical behavior in unloading conditions of sandstone after high-temperature treatment. *Rock Mechanics and Rock Engineering, 49*(7), 2641–2653.

Duchane, D., & Brown, D. (2002). Hot dry rock (HDR) geothermal energy research and development at Fenton Hill, New Mexico. GHC Bulletin December; 2002. pp. 13–9.

Fan, L. F., Gao, J. W., Wu, Z. J., Yang, S. Q., & Ma, G. W. (2018). An investigation of thermal effects on micro-properties of granite by X-ray CT technique. *Applied Thermal Engineering, 140,* 505–519.

Feng, G., Yong, K., Meng, T., Hu, Y. Q., & Li, X. H. (2017). The influence of temperature on mode I fracture toughness and fracture characteristics of sandstone. *Rock Mechanics and Rock Engineering, 50*(8), 2007–2019.

Fox, D. B., Sutter, D., Beckers, K. F., Lukawski, M. Z., Koch, D. L., Anderson, B. J., & Tester, J. W. (2013). Sustainable heat farming: Modeling extraction and recovery in discretely fractured geothermal reservoirs. *Geothermics, 46*(4), 42–54.

Frash, L. P., Gutierrez, M., Hampton, J., & Hood, J. (2015). Laboratory simulation of binary and triple well EGS in large granite blocks using AE events for drilling guidance. *Geothermics, 55,* 1–15.

Gao, J., Zhang, H. J., Zhang, S. Q., Chen, X. B., Cheng, Z. P., Jia, X. F., et al. (2018). Three-dimensional magnetotelluric imaging of the geothermal system beneath the Gonghe Basin, Northeast Tibetan Plateau. *Geothermics, 76,* 15–25.

Glover, P. W. J., Baud, P., Darot, M., Meredith, P. G., Boon, S. A., LeRavalec, M., et al. (1995). $\alpha/\beta$ phase transition in quartz monitored using acoustic emissions. *Geophysical Journal of the Royal Astronomical Society, 120*(3), 775–782.

Gónzalez-Gómez, W. S., Quintana, P., May-Pat, A., Avilés, F., May-Crespo, J., & Alvarado-Gil, J. J. (2015). Thermal effects on the physical properties of limestone from the Yucatan Peninsula. *International Journal of Rock Mechanics & Mining Sciences, 75,* 182–189.

Han, G. S., Jing, H. W., Su, H. J., Liu, R. C., Yin, Q., & Wu, J. Y. (2019). Effects of thermal shock due to rapid cooling on the mechanical properties of sandstone. *Environmental Earth Sciences, 78*(5), 146.

Hoek, E., & Brown, E. T. (1980). Empirical strength criterion for rock masses. *Journal of the Geotechnical Engineering Division, 106*(15715), 1013–1035.

Huang, X., Liu, Q. S., Liu, B., Liu, X. W., & Pan, Y. C. (2017). Experimental study on the dilatancy and fracturing behavior of soft rock under unloading conditions. *International Journal of Civil Engineering, 15,* 921–948.

Jiang, G. H., Zuo, J. P., Li, Y. L., & Wei, X. (2019). Experimental investigation on mechanical and acoustic parameters of different depth shale under the effect of confining pressure. *Rock Mechanics and Rock Engineering, 52*(11), 4273–4286.

Jin, P. H., Hu, Y. Q., Shao, J. X., Zhao, G. K., Zhu, X. Z., & Li, C. (2019). Influence of different thermal cycling treatments on the physical, mechanical and transport properties of granite. *Geothermics, 78,* 118–128.

Kumari, W. G. P., Beaumont, D. M., Ranjith, P. G., Perera, M. S. A., Isaka, B. L. A., & Khandelwal, M. (2019). An experimental study on tensile characteristics of granite rocks exposed to different high-temperature treatments. *Geomechanics and Geophysics for Geo-Energy and Geo-Resources, 5*(1), 47–64.

Labuz, J. F., Zang. A. (2012). Mohr–Coulomb Failure Criterion. *Rock Mechanics & Rock Engineering*, *45*(6), 975–979.

Lau, J. S. O., & Chandler, N. A. (2004). Innovative laboratory testing. *International Journal of Rock Mechanics & Mining Sciences, 41*(8), 1427–1445.

Li, D. Y., Sun, Z., Xie, T., Li, X. B., & Ranjith, P. G. (2017). Energy evolution characteristics of hard rock during triaxial failure with different loading and unloading paths. *Engineering Geology, 228,* 270–281.

Liang, Y. P., Li, Q. M., Gu, Y. L., & Zou, Q. L. (2017). Mechanical and acoustic emission characteristics of rock: Effect of loading and unloading confining pressure at the postpeak stage. *Journal of Natural Gas Science and Engineering, 44,* 54–64.

Liu, S., & Xu, J. (2015). An experimental study on the physico-mechanical properties of two post-high-temperature rocks. *Engineering Geology, 185,* 63–70.

Mahanta, B., Singh, T. N., & Ranjith, P. G. (2016). Influence of thermal treatment on mode I fracture toughness of certain Indian rocks. *Engineering Geology, 210,* 103–114.

Meng, L. B., Li, T. B., Liao, A. J., & Zeng, P. (2018). Anisotropic mechanical properties of sandstone under unloading confining pressure at high temperatures. *Arabian Journal for Science & Engineering, 43,* 5283–5294.

Mohamadi, M., & Wan, R. G. (2016). Strength and post-peak response of Colorado shale at high pressure and temperature. *International Journal of Rock Mechanics & Mining Sciences, 84,* 34–46.

Nasseri, M. H. B., Schubnel, A., & Young, R. P. (2007). Coupled evolutions of fracture toughness and elastic wave velocities at high crack density in thermally treated Westerly granite. *International Journal of Rock Mechanics & Mining Sciences, 44,* 601–616.

Peng, J., Rong, G., Cai, M., Tao, M. D., & Zhou, C. B. (2016). Comparison of mechanical properties of undamaged and thermal-damaged coarse marbles under triaxial compression.

*International Journal of Rock Mechanics & Mining Sciences, 83,* 135–139.

Pranay, A., Palash, P., John, M. L., & Joseph, M. (2019). Efficient workflow for simulation of multifractured enhanced geothermal systems (EGS). *Renewable Energy, 131,* 763–777.

Qiu, S. L., Feng, X. T., Xiao, J. Q., & Zhang, C. Q. (2014). An experimental study on the pre-peak unloading damage evolution of marble. *Rock Mechanics & Rock Engineering, 47*(2), 401–419.

Rong, G., Peng, J., Yao, M. D., Jiang, Q. H., & Wong, L. N. Y. (2018). Effects of specimen size and thermal-damage on physical and mechanical behavior of a fine-grained marble. *Engineering Geology, 232,* 46–55.

Rathnaweera, T. D., Ranjith, P. G., Gu, X., Perera, M. S. A., Kumari, W. G. P., Wanniarachchi, W. A. M., et al. (2018). Experimental investigation of thermomechanical behaviour of clay-rich sandstone at extreme temperatures followed by cooling treatments. *International Journal of Rock Mechanics & Mining Sciences, 107,* 208–223.

Schindelin, J., Arganda-Carreras, I., Frise, E., Kaynig, V., Longair, M., Pietzsch, T., et al. (2012). Fiji: an open-source platform for biological-image analysis. *Nature Methods, 9*(7), 676–682.

Shen, Y. J., Zhang, Y. L., Gao, F., Yang, G. S., & Lai, X. P. (2018). Influence of Temperature on the Microstructure Deterioration of Sandstone. *Energies, 11*(7), 1753.

Singh, B., Ranjith, P. G., Chandrasekharam, D., Viete, D., Singh, H. K., & Lashin, A. (2015). Thermo-mechanical properties of Bundelkhand granite near Jhansi, India. *Geomechanics and Geophysics for Geo-Energy and Geo-Resources, 1,* 35–53.

Siratovich, P. A., Heap, M. J., Villeneuve, M. C., Cole, J. W., Kennedy, B. M., Davidson, J., & Reuschlé, T. (2016). Mechanical behaviour of the Rotokawa Andesites (New Zealand): Insight into permeability evolution and stress-induced behaviour in an actively utilised geothermal reservoir. *Geothermics, 64,* 163–179.

Somerton, W. H. (1993). Thermal properties and temperature related behaviour of rock/fluid systems. *Journal of Volcanology & Geothermal Research, 56*(1–2), 171–172.

Tian, H., Ziegler, M., & Kempka, T. (2014). Physical and mechanical behavior of claystone exposed to temperatures up to 1000 °C. *International Journal of Rock Mechanics & Mining Sciences, 70,* 144–153.

Ulusay, R., & Hudson, J.A. (2007). The complete ISRM suggested methods for rock characterization, testing and monitoring: 1974–2006. Commission on testing methods, International Society of Rock Mechanics, Compilation arranged by the ISRM Turkish National Group, Ankara, Turkey.

Wang, F., Frühwirt, T., & Li, Y. (2020). The influence of temperature and high-speed heating on tensile strength of granite and the application of digital image correlation on tensile failure processes. *Rock Mechanics and Rock Engineering, 53*(4), 1935–1952.

Wu, Q. H., Weng, L., Zhao, Y. L., Guo, B. H., & Luo, T. (2019a). On the tensile mechanical characteristics of fine-grained granite after heating/cooling treatments with different cooling rates. *Engineering Geology, 253,* 94–110.

Wu, X. G., Huang, Z. W., Song, H. Y., Zhang, S. K., Cheng, Z., Li, R., et al. (2019b). Variations of physical and mechanical properties of heated granite after rapid cooling with liquid nitrogen. *Rock Mechanics and Rock Engineering, 52*(7), 2123–2139.

Yang, S. Q., Xu, P., Li, Y. B., & Huang, Y. H. (2017). Experimental investigation on triaxial mechanical and permeability behavior of sandstone after exposure to different high temperature treatments. *Geothermics, 69,* 93–109.

Yang, S. Q., Tian, W. L., Elsworth, D., Wang, J. G., & Fan, L. F. (2020). An experimental study of effect of high temperature on the permeability evolution and failure response of granite under triaxial compression. *Rock Mechanics and Rock Engineering, 53,* 4403–4427.

Yu, K. F., Zhou, Y. J., Liu, Y. L., Liu, F. S., Hu, L. P., Ao, W. Q., et al. (2020). Near-room-temperature thermoelectric materials and their application prospects in geothermal power generation. *Geomechanics and Geophysics for Geo-Energy and Geo-Resources, 6*(1), 1–12.

Zhang, W. Q., Sun, Q., Hao, S. Q., Geng, J. S., & Lv, C. (2016). Experimental study on the variation of physical and mechanical properties of rock after high temperature treatment. *Applied Thermal Engineering, 98,* 1297–1304.

Zhang, Y. J., Ma, Y. Q., Hu, Z. J., Lei, H. L., Bai, L., Lei, Z. H., & Zhang, Q. (2019). An experimental investigation into the characteristics of hydraulic fracturing and fracture permeability after hydraulic fracturing in granite. *Renewable Energy, 140,* 615–624.

Zhao, G. Y., Dai, B., Dong, L. J., & Chen, Y. (2015). Energy conversion of rocks in process of unloading confining pressure under different unloading paths. *Transactions of Nonferrous Metals Society of China, 25*(5), 1626–1632.

Zhu, Z. N., Tian, H., Jiang, G. S., & Cheng, W. (2018). Effects of high temperature on the mechanical properties of chinese marble. *Rock Mechanics and Rock Engineering, 51*(6), 1937–1942.

Zhu, Z., Tian, H., Chen, J., Jiang, G. S., Dou, B., Xiao, P., & Mei, G. (2020). Experimental investigation of thermal cycling effect on physical and mechanical properties of heated granite after water cooling. *Bulletin of Engineering Geology and the Environment, 79,* 2457–2465.